International Journal of Engineering

Journal Homepage: www.ije.ir

Determination of Shock Standoff Distance for Wedge at Supersonic Flow

A. Mishra*[a], A. Khan[b], N. Musfirah Mazlan[b]

[a] *Department of Aerospace Engineering, IIT Kanpur, India*
[b] *School of Aerospace Engineering, Engineering Campus, Universiti Sains Malaysia, Pulau Pinang, Malaysia*

PAPER INFO

Paper history:
Received 05 February 2019
Received in revised form 12 March 2019
Accepted 02 May 2019

Keywords:
Flow Channel
Shock Standoff
Supersonic Flow
Wedge

ABSTRACT

An experimental investigation is conducted to calculate the shock standoff (SSO) distance in front of an acute-angled wedge. For this experimentation, simple water flows channel analysis is carried out. The flow velocity is varied from 13.2 cm/s to 25.5 cm/s increasing in steps of 1 cm/s. A velocity of 13.2 cm/s corresponds to Froude number 1.13 and velocity of 25.5 cm/s to Froude number 1.41. The Froude number ranged from 1.13 to 1.41 in steps of 0.04. The study is conducted on 5 mm thick acrylic sheets and of wedge angles 50°, 60°, and 75° to obtain a relation for calculating the SSO distance concerning the Froude number. It is found that the pressure uphill strongly depends upon the Fr and wedge angle. The SSO distance determined experimentally and using the proposed correlation are found to be in good agreement.

***doi**: 10.5829/ije.2019.32.07a.19*

1. INTRODUCTION

The flow of fluid over a blunt body and a sphere is studied since past many decades and is considered a fundamental topic in the area of fluid dynamics. Experimental and numerical investigations in large amount are accessible as basic research in this exciting field of high speed flows pertinent to drag, shock waves, and vortex shedding. [1,2]. The occurrence of shock waves near the blunt/spherical geometries of aerodynamic vehicles also causes the increased temperature of the fluid behind the shock due to compression. The distance between the shock front and the surface of aerodynamic geometry is known as shock stand-off (SSO) distance and is calculated along the propagation axis. This distance has a strong dependence on fluid flow conditions and is studied extensively, along with its associated phenomena are focused. In few cases of high speed flows, due to the reduction in temperature of fluid molecules, the SSO distance reduces and hence act as necessary reference quantities in high-speed flows [3], [4,5]. Understanding the development of shock waves and its standoff distance from the aerodynamic geometry is of particular importance in space transport and projectile systems. Some ideas/modifications are implemented by various scientists to alter the fluid flow near the aerodynamic shapes by using passive control and active control devices. Use of spikes is the best example of passive control as it changes a strong shock into a weak foreshock [6,7].

Various experimental studies assisted by numerical analysis are pertinent to shock waves, vortex shedding, drag, standoff distance, and pressure fluctuations around aerodynamic shapes. Farris and Russel [2] determined the SSO distance of bow shock which is influenced by the size/shape of the body, magnetic field orientation, magnetosonic Mach number, and plasma beta. A correlation was established between bow SSO distance and Mach number. Solar wind dynamic pressure is found to have enough impact on bow SSO distance. Cairns and Lyon [8] analyzed the effect of orientation of the magnetic field on bow SSO distance of earth. The orientation was found to have a good impact on bow SSO distance for Mach<10, and for lower Mach, the shock moves closer to earth with no orientation of magnetic field. Houwing et al. [9] for non-equilibrium flows checked the impact of vibrational relaxation

*Corresponding Author Email: *superavinashtunnel@gmail.com* (A. Mishra)

Please cite this article as: A. Mishra, A. Khan, N. Musfirah Mazlan, Determination of Shock Standoff Distance for Wedge at Supersonic Flow, International Journal of Engineering (IJE), IJE TRANSACTIONS A: Basics Vol. 32, No. 7, (July 2019) 1049-1056

behind the bow SSO distance from the sphere. Flow parameters which affect the SSO distance for correlating the experimental data are confirmed in their work [9]. Nonaka et al. [10] measured SSO distance at hypersonic regime for the sphere in a ballistic range. For different nose radius and speed of 2.44 km/s to 3.85 km/s of the flight at 5600-20000 Pa. The visualization of the flow was done using schlieren method and light source from an Nd-YAG laser. The SSO distance was found to be larger due to gas contamination effect [10]. In cold spray processes, a formation of the bow shock is seen between the substrate and the jet during smaller SSO distance, studied by Pattison et al. [11]. Using aluminum, titanium, copper powder, and helium nozzle functioning at 20˚C and 2 MPa along with nitrogen nozzle at 300°C and 3 MPa experiments were carried. The deposition efficiency and SSO distance were found to have a relation such that at a distance of <60 mm, deposition efficiency was reduced by the shock around 40% [11]. Hashimoto et al. [4] analyzed the influence of hemispherical model radius, flow velocity, and flow density in a ballistic range on SSO distance. Kikuchi et al. [12] estimated the SSO distance for flow at transonic speed over a sphere.

Itoh et al. [5] considered the hypersonic regime to understand the parameters affecting SSO distance over a blunt object. With an understanding of the rate of chemical reaction and the SSO distance being closely related along the line of propagation, the impact of sphere nose radius was investigated. It was found that SSO distance helps in understanding the number of atoms of oxygen in the stream of the shock tunnel. Igra and Falcovitz [13] numerically simulated the bow SSO distance at supersonic regime over the sphere in Mach number varying from 1.025 to 1.2. Using the turbulence model of Spalart–Allmaras viscous flow simulations were shown. Saito et al. [3] analyzed the SSO distance over a sphere decelerating with transonic speed. Numerical codes were employed for the measurement of SSO distance and found that the viscous effects to be marginal which can be neglected and required less computational time. Savani et al. [14] carried numerical simulations of magnetohydrodynamic in 2.5D (dimensions) of shock and CMEs. The effect on SSO distance as a function of the radial half width of CME (coronal mass ejections) was investigated. The SSO distance is found to vary proportionally with heliocentric distance and radius of CMEs edge. Zander et al. [15] measured the SSO distance at hypersonic flows over a sphere. The speed of 9.7 km/s and 8.7 km/s were operated in expansion tunnel having a nozzle of Mach 10. Image captured using a high-speed camera and least square (shape fitting algorithm) the data was analyzed. Sinclair and Cui [16] attempted successfully to determine SSO distance at all Mach values theoretically. Numerical analysis was also performed to validate the relation developed for approximating the SSO distance based on the Newtonian impact theory. The results obtained by both methods were found in good agreement. Wang et al. [17] experimented to determine the SSO distance over a forward facing cylinder step with the flow at Mach 10. High-speed video was recorded, and the pressure transducer was used for measurements. The change in entropy with shock shape were obtained to know the entropy distribution. The extreme values shifted mostly close to the flat-faced nose than the blunt nose with an increase in Mach number, as the flat faced shape influences the shock shape more than the blunt shape.

Other studies related to the above discussion is reported by Gopalswamy et al. [18] on the circular profile from the SSO distance of coronal magnetic field, Zhang et al. [19] on shock wave reflection over a wedge, and Poomvises et al. [20] on radial magnetic field of a CME driven shock from the SSO distance. Rathakrishnan and his team reported many studies carried using water channel experiment for visualization of flow over a blunt body, flat plate, and blunt body with a spike. Vortex shedding, shock wave analysis, and pressure uphill movements were thoroughly analyzed [6,7,21–23], and several other [24–26]. Thus it is clear from these studies that SSO distance measurement over a wedge is not carried out. Several studies are found on SSO distance measurement using the analytical, experimental and numerical method at different flow regimes whereas none over wedge body are reported. Hence an attempt is made to determine the SSO distance over the wedge using a water channel experiment and relation is developed between the SSO distance and flow velocity.

2. BACKGROUND

2. 1. Shock Standoff Distance The ratio of density ($\rho 1/\rho 2$), across the shock has an essential effect on the shock detachment distance in front of a blunt-nosed body in hypersonic flow. An approximate expression for the shock detachment distance (δ), ahead of the nose of a blunt-nosed body, with a round nose of radius (R), regarding density ratio across the detached shock, is given by Equation (1).

$$\frac{\delta}{R} = \frac{\frac{\rho_1}{\rho_2}}{1+\sqrt{2(\frac{\rho_1}{\rho_2})}} \quad (1)$$

Here, $\rho 1$ is the density for a fluid with M>1 and ρ2 is the density for a fluid with M<1. In the limit of high velocities, the density ratio $\rho 1/\rho 2$ becomes small compared to unity, and Equation 1 is approximated by Equation (2).

$$\frac{\delta}{R} \approx \frac{\rho_1}{\rho_2} = \frac{1}{\left(\frac{\rho_2}{\rho_1}\right)} \quad (2)$$

Therefore, the value of the density ratio $\rho 1/\rho 2$ across a standard shock has a significant impact on shock detachment distance; the higher the density ratio, $\rho 1/\rho 2$, is, the smaller is the shock detachment distance, δ.

2. 2. Detached Shock Waves When the wall deflection angle $\theta > \theta_{max}$, the shock waves appear to be detached from the surface as shown in Figure 1. From the experiments, it is found that for the fluid flow having deflection $\theta > \theta_{max}$ the profile of shock appears as shown in Figure 1. The distance of the shock depends on the shape of the object facing the flow, and it's Mach number. The wedge geometry gives the flow an acceleration to supersonic flow from the subsonic flow; hence there is an occurrence of a sonic line originating from the wedge shoulder as shown in Figure 1 (a). This sonic line in blunt bodies is often complicated to locate [27,28], [29].

3. THE WATER CHANNEL EXPERIMENT

The water flow through an open channel has a simple duct where water flows with constant velocity over the entire length of the channel. This open channel length has the object over which the water flows and visualization are carried out. The schematic view of a rectangular duct for water flow is shown in Figure 2. The water from chamber flows over the horizontal plate (open duct) and is streamlined by flowing through some wire meshes (screens) as shown in Figure 2 (a). These screens are used to ensure a uniform flow of water over the test section. For better understanding and visualization of the flow field over the wedge (test section), the color dye is injected before the screens. Hence these screens streamline/condition the flow of water and the smooth parallel dye streaks over the test object help in clear flow visualization. Using the floating-particle method technique, the velocity of water flow is calculated along the length of the object.

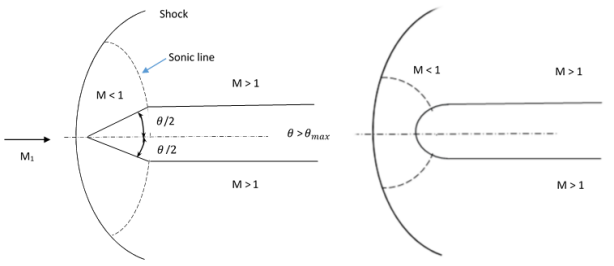

(a) wedge for $\theta > \theta_{max}$ (b) blunt body

Figure 1. Detached shock waves over the wedge and blunt nose

The duct is of 300 mm width and has a depth of 6 mm. A wedge model of side length 30 mm and 5 mm thickness of different wedge angles (50°, 60°, and 75° as shown in Figure 3) is placed with wedge towards the flow. The wedge as a test section is placed on the flat horizontal part of the duct and is fixed to it such that no water passes through the bottom of the wedge. Hence the flow can be considered to be two dimensional having an open free surface. The wedge is placed at the mid of the section and acrylic color dye is injected before the screens. The boundary layer of the flow did not show any effect on flow uniformity which is observable. The temperature of the water flow is almost constant, with a maximum variation of ±0.5°C, during experiments. The flow direction is parallel to the bottom and side surfaces of the water flow channel, with a maximum deviation of about ±1°. The wedge is placed, with their length, normal to the flow direction with a maximum deviation of ±1°. The lens of the video camera is held parallel and directly above the model. The 30˚C temperature of the water is kept constant, and the video recording is done using a Panasonic DMC-II model having a resolution of 1280x720 operating at a

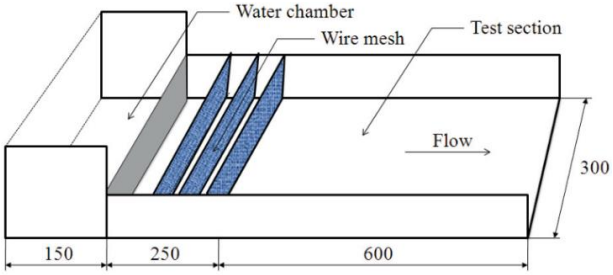

(a) Schematic view of the water channel

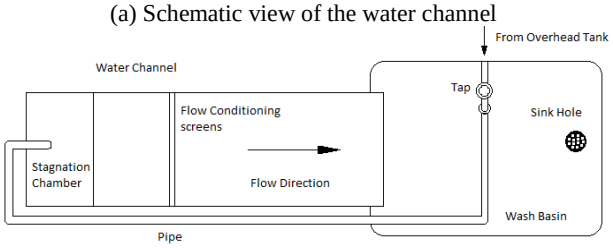

(b) Top view of the setup

Figure 2. Experimental employed for the SSO distance visualization

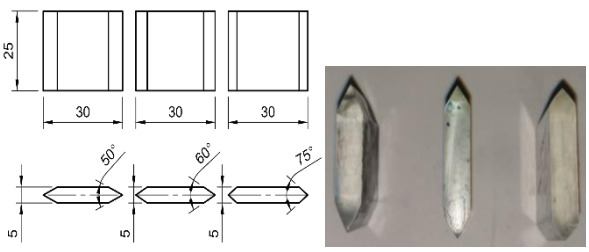

Figure 3. Wedges used to analyze the flow deflection

speed of 120 frames/s. The video which was recorded during the experiments provide a proper image of stagnation point and shock occurrence as shown in Figure 4. A plate with measurements marked is used to calculate the pressure uphill distance in front of the wedge having a thickness of 5mm. The shock standoff distance is later calculated from this data by employing suitable assumptions.

The uniformity of the flow is of prime importance, and it is analyzed by observing the movement of the floating body like a tiny paper. This paper is moved from the start to the last point of the channel. The parallel and straight movement of the paper confirms the flow uniformity along the channel and sidewalls. The streak lines of the flow at the side channel walls and the test object were also seen to be uniform. After this test of flow uniformity, the velocity of water is calculated by recording the time taken by the paper to cover the distance along the channel. For each velocity, many readings are taken, and then the average of the data is considered for the flow. The required velocity is arrived by operating the test section which is within the velocity limit of the water channel. Using smoke, surface coating, and tuft the physics of flow in several exciting aspects can be easily visualized. However, this is not feasible for all the flows and hence using the above setup of a water channel and using water visualization can be made. With the help of hydraulic analogy, even some aspects of supersonic and even hypersonic flow can be studied by matching the Froude number of the water channel flow to the desired Mach number.

4. RESULTS AND DISCUSSION

The study of Froude number (Fr) in the water flow having a free surface as in this water channel is similar to the flow of gas with Mach number [1].

Figure 4. A view of the flow pattern around the wedge model

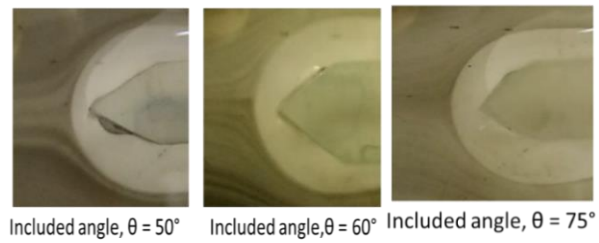

(a) Fr 1.13

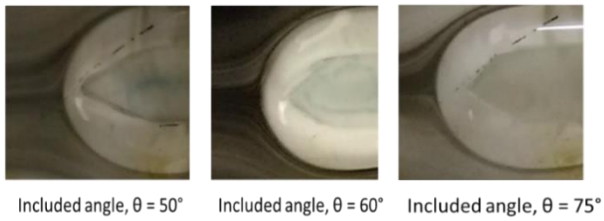

Fr 1.17

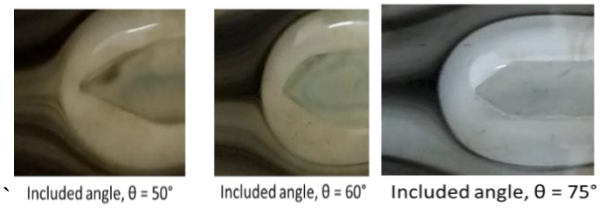

Fr 1.21

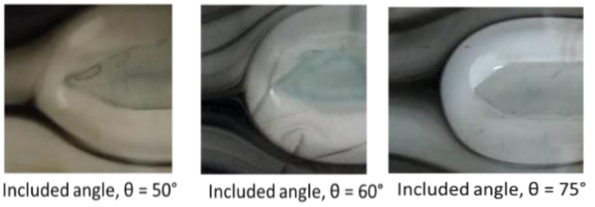

Fr 1.25

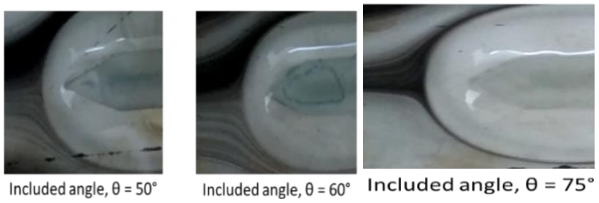

Fr 1.29

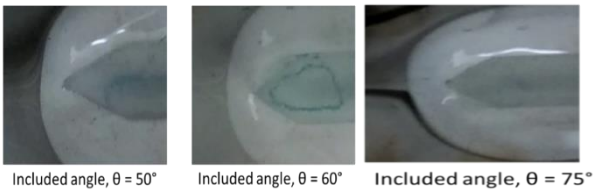

Fr 1.33

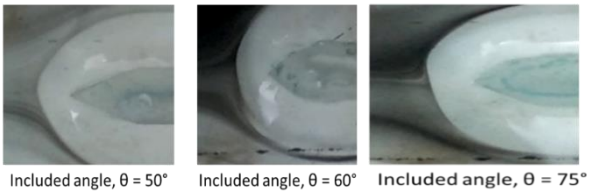

Fr 1.37

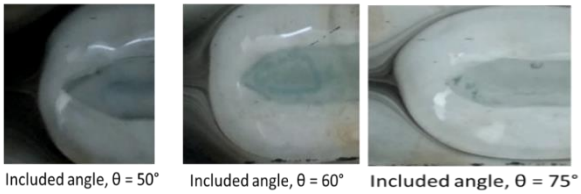

Fr 1.41

Figure 5. Pressure uphill in front of the wedge for Fr 1.13 to Fr 1.41

Fr is the ratio of the speed of fluid to the characteristics speed of flow in a shallow water channel while Mach number represents the ratio of the speed of a body to speed of sound in surrounding media. The extent of pressure uphill and SSO distance as a function of Mach (here Froude) number and wedge angle is discussed quantitatively in this section. The flow of water over wedge is parallel to the free stream with velocities varied from 13.2 cm/s to 25.5 cm/s increasing in steps of 1 cm/s. The velocity of 13.2 cm/s corresponds to Froude number 1.13 and velocity of 25.5 cm/s to Froude number 1.41. This Froude number chosen in this study is analogous to the supersonic flow of air. Hence the analysis provided using water channel flow helps to correlate the flow behavior with air with a simple and feasible experiment.

4. 1. Pressure Uphill Variation In literature, no information of SSO distance over the wedge is available, and this investigation reports the same. For wedge included angles of 50˚, 60˚, and 75˚ and Fr variation from 1.13 to 1.41 in steps of 0.04 the pressure uphill in front of the wedge is shown in Figure 5 (a) – (f) respectively. In Figure 5 the streamlines of the flow field at Fr 1.13 is shown for three different included angles of the wedge. The size of the streamlines deflected in front of the wedge is seen to increase in its width with improvement in the angle of the wedge. The change in curvature of streamlines is observed with the included angle of the wedge. These streamlines are pushed away by a positive zone of pressure in front of the wedge sharp edge. This pressure zone notably known by pressure uphill has a certain width and changes with flow velocity, i.e., Fr. Hence the streamlines curvature has a strong dependence upon the width of the pressure uphill. This size of this pressure uphill is found to monotonically increase with increment in velocity (Fr) of the flow as shown in Figure 5 (b) – (f). Once the streamlines find a pressure zone ahead of flow direction, they take a turn to negotiate the pressure uphill. Once they cross this zone the streamlines once again start flowing parallel to the wedge as there is no much fluctuations and significant vortex formation in the flow field.

4. 2. Pressure Uphill Ratio The distance of pressure uphill from the wedge obtained by the experimentation and visualized through the computer software by the method of pixel location difference is studied with variation in Fr and half wedge angle. A correlation is developed for the SSO distance and pressures uphill distance (PUD) wherein it is hypothesized that the SSO distance is a function of flow Froude number, maximum deviation angle, half wedge angle, (here fictitious) density ratio. In the range of Fr operated for the flow, the PUD is found to change monotonously with Fr as discussed previously. This result also agrees with the literature works already known to us. The experimental results consist of the video of the flow field over the wedges of half-wedge angle 25˚, 30˚, and 37.5˚ at eight Froude numbers (1.13 to 1.41 in steps of 0.04). The flow physics behind the formation of the detached shock has already been discussed.

The variation of the ratio of pressure uphill at different Fr and pressure uphill at maximum deviation angle which is known as uphill pressure ratio is plotted against Fr shown in Figure 6. As explained earlier, the pressure uphill monotonously increases with Fr and the wedge angle, the same is shown in Figure 6 (a) – (c) for each wedge angle slight fluctuation is seen. However, the trend keeps increasing showing the improvement in strength of pressure uphill. At wedge angle of 25˚, the uphill pressure ratio is of lesser value compared to 30˚ and 37.5˚ at Fr 1.13. Further, with enhancement in Fr, this ratio remained increasing irrespective of any angle. However, the increase in this ratio at 25˚ is lesser at higher Fr then at 30˚ and 37.5˚. The highest value of pressure uphill ratio reached is 0.44 at Fr 1.41 for 25˚, and it was 0.57 and 0.74 at Fr 1.14 for 30˚ and 37.5˚ respectively as illustrated in Figure 6 (b) and (c). Thus it can be concluded that the pressure uphill drastically increases with increase in Fr and wedge angle.

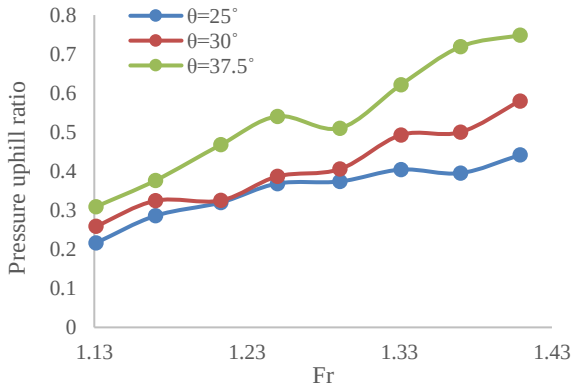

Figure 6. PHR variation with Fr and Δθ ratio at different semi-wedge angles

The ratio of pressure uphill distance (PUD) and calculated SSO distance vs. Fr is depicted in Figure 7 (a) to (c) for different wedge angles. Precisely as expected the nature of trend is more or less about a mean value of 0.75 for all Fr. The above trend clearly shows that both (pressure uphill and SSO distance) increase with an increase in Fr. The mean value is slightly increased to 0.8 and 0.85 at all Fr for wedge angle of 30˚ and 37.5˚ respectively on Figure 7 (b) and (c). The improvement in this ratio of SSO and pressure uphill distance is in agreement with the previous conversation of pressure uphill variation with Fr.

4. 3. SSO Distance Measurement The PUD for the wedge is obtained using by the method of pixel difference location on an extracted image. Since it is hypothesized that their ratio was a constant, the SSO distance relation with Froude number is formulated by employing suitable assumptions. The correlation hence derived is given below. The hypothesized formulae for the SSO distance is given by for any wedge angle θ [16],

$$\delta_c = \delta_{c,max}(Fr-1)^l \left(\frac{\theta-\theta_{max}}{\pi-\theta_{max}}\right)^m \left(\frac{1}{ln(\frac{2}{\rho_1/\rho_2-1})}\right)^n \quad (3)$$

The maximum SSO distance occurs for θ = π, hence:

$$\delta_{c,max} = 7.1(Fr-1)^{0.463} \quad (4)$$

The proposed correlations for the wedge angles are as follows: For wedge 50°

$$\delta_c = \delta_{c,max}(Fr-1)^{0.21} \left(\frac{\theta-\theta_{max}}{\pi-\theta_{max}}\right)^{0.165} \left(\frac{1}{ln(\frac{2}{\rho_1/\rho_2-1})}\right)^{0.435} \quad (5)$$

For wedge 60°,

$$\delta_c = \delta_{c,max}(Fr-1)^{0.21} \left(\frac{\theta-\theta_{max}}{\pi-\theta_{max}}\right)^{0.2} \left(\frac{1}{ln(\frac{2}{\rho_1/\rho_2-1})}\right)^{0.691} \quad (6)$$

For wedge 75°,

$$\delta_c = \delta_{c,max}(Fr-1)^2 \left(\frac{\theta-\theta_{max}}{\pi-\theta_{max}}\right)^0 \left(\frac{1}{ln(\frac{2}{\rho_1/\rho_2-1})}\right)^{1.222} \quad (7)$$

The variation in SSO distance with Fr is shown in Figure 8-10 for the half-wedge angle of 25˚, 30˚, and 37.5˚ respectively. It is clear from Figure 8-10 that with increasing Fr the SSO distance increases. Similarly, the SSO distance increases with the wedge angle as well which is again in agreement with the earlier results. The SSO distance obtained from the correlation developed and the experimental (actual) distance look in agreement. Hence the proposed correlation is helpful in the prediction of SSO distance ahead of the wedge for different Fr. Also, the proposed correlation works as a function of wedge angle and density ratio. Further analysis can be theoretically made based on the above-proposed relation. The hydraulic analogy worked here for simple experimental determination of SSO distance as a function of flow velocity (Fr) which is Mach number in case of a gas flow.

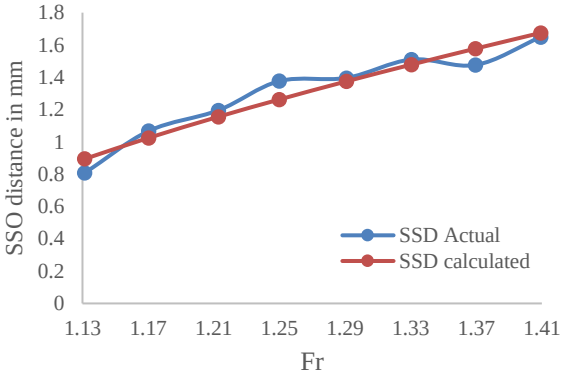

Figure 8. SSO distance variation with Fr by proposed (calculated) and actual at 25˚

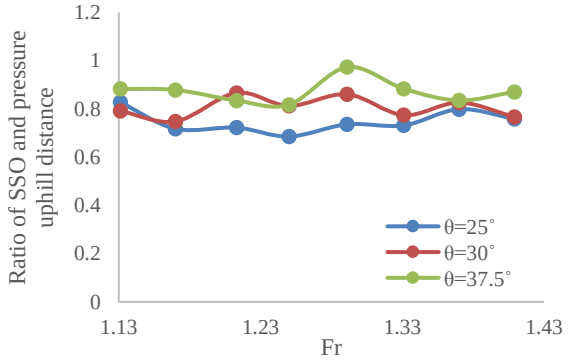

Figure 7. The ratio of PUD and calculated SSO distance vs. Fr at different semi-wedge angles

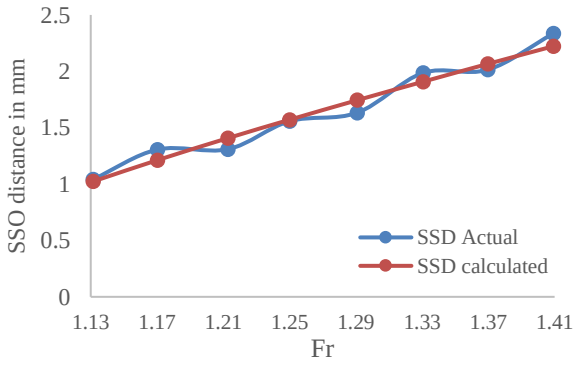

Figure 9. SSO distance variation with Fr by proposed (calculated) and actual at 30˚

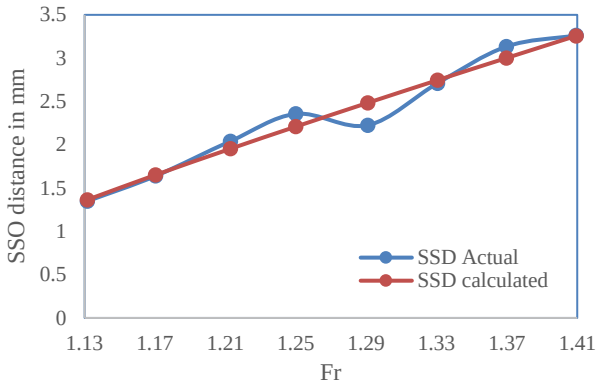

Figure 10. SSO distance variation with Fr by proposed (calculated) and actual at 37.5˚

4. CONCLUSION

The flow around a wedge positioned parallel to the flow was visualized over a range of Froude numbers (Fr) which were higher than 1 and hence analogous to supersonic flow in the air. The pressure uphill distance varies monotonously with the Froude number. The results strongly suggested that the ratio of the pressure uphill distance and shock standoff distance is almost constant. The SSO distance was found to be a function of Froude number and half-wedge angle. Quantitative relations were formulated to calculate the shock standoff distance in front of a wedge. The pressure uphill is found to increase with Fr and wedge angle drastically. In future the following works need to be carried out to get an insight of SSO and pressure uphill variations:

1. The above work can be extended to include Froude numbers higher than 1.45 and semi-wedge angles from 1° to 89°.
2. Relations have to be formulated to check the functional dependence of SSD on parameters included in the above study.
3. Numerical studies will provide validation of the results and in-depth simulation of SSD variations.

5. REFERENCES

1. E. Rathakrishnan, Instrumentation, measurements, and experiments in fluids. CRC Press, 2007.
2. Farris, M. H., and C. T. Russell. "Determining the standoff distance of the bow shock: Mach number dependence and use of models." ***Journal of Geophysical Research: Space Physics***, Vol. 99, No. A9, (1994), 17681-17689.
3. T. Saito, K. Hatanaka, H. Yamashita, T. Ogawa, S. Obayashi, and K. Takayama, "Shock stand-off distance of a solid sphere decelerating in transonic velocity range," ***Shock Waves***, Vol. 21, No. 5 (2011) 483–489.
4. T. Hashimoto, T. Komuro, K. Sato, and K. Itoh, "Experimental investigation of shock stand-off distance on spheres in hypersonic nozzle flows," ***Shock Waves***, (2009), 961–966.
5. K. Itoh et al., "Flow Characterization of High Enthalpy Shock Tunnel Based on Shock Stand-off Distance," in International Space Planes and Hypersonic Systems and Technologies Conference, (2009), 1–8.
6. S. Khurana, K. Suzuki, and E. Rathakrishnan, "Flow Field around a Blunt-nosed Body with Spike," ***International Journal of Turbo Jet Engines,*** Vol. 29, (2012) 217–221.
7. S. Khurana and K. Suzuki, "Assessment of Aerodynamic Effectiveness for Aerospike Application on Hypothesized Lifting-Body in Hypersonic Flow," in Fluid Dynamics and Co-located Conferences, (2013), 24–27.
8. Cairns, Iver H., and J. G. Lyon. "Magnetic field orientation effects on the standoff distance of Earth's bow shock." ***Geophysical Research Letters,*** Vol. 23, No. 21 (1996), 2883-2886.
9. A. F. P. Houwing, S. Nonaka, and H. Mizuno, "Effects of Vibrational Relaxation on Bow Shock Standoff Distance for Nonequilibrium Flows," ***AIAA Journal***, Vol. 38, No. 9, (1999) 1760–1763,
10. S. Nonaka, H. Mizuno, K. Takayama, and C. Park, "Measurement of Shock Standoff Distance for Sphere in Ballistic Range," ***Journal of Thermophysics and Heat Transfer,*** Vol. 14, No. 2 (2000): 225-229.
11. J. Pattison, S. Celotto, A. Khan, and W. O. Neill, "Standoff distance and bow shock phenomena in the Cold Spray process," ***Surface and Coatings Technology,*** Vol. 202, No. 8 (2008): 1443-1454.
12. T. Kikuchi, D. Numata, K. Takayama, and M. Sun, "Shock stand-off distance over spheres flying at transonic speed ranges in the air," ***Shock Waves***, (2009) 515–520.
13. D. Igra and J. Falcovitz, "Shock wave standoff distance for a sphere slightly above Mach one," ***Shock Waves***, Vol. 20, (2010), 441–444.
14. N. P. Savani, D. Shiota, K. Kusano, A. Vourlidas, and N. Lugaz, "A study of the Heliocentric dependence of Shock Standoff Distance and Geometry using 2. 5D MHD Simulations of CME-driven shocks," ***The Astrophysical Journal***, Vol. 759, No. 2, (2012), doi: 10.1088/0004-637X/759/2/103.
15. F. Zander, R. J. Gollan, P. A. Jacobs, and R. G. Morgan, "Hypervelocity shock standoff on spheres in air," ***Shock Waves***, Vol. 24, (2014), 171–178.
16. J. Sinclair and X. Cui, "A theoretical approximation of the shock standoff distance for supersonic flows around a circular cylinder" Phys. Fluids, Vol. 29, (2017), https://doi.org/10.1063/1.4975983.
17. Wang, G., Yang, Y., Ma, X., Jiang, T., Gong, H. and Kong, R., "Prediction of Shock-Standoff Distance and Entropy Distribution for Forward-Facing Cavity" ***International Journal of Astrophysics and Space Science,*** Vol. 6 No. 3, (2018), 52-61.
18. N. Gopalswamy and S. Yashiro, "The Strength and Radian Profile of the Coronal Magnetic Field from the Standoff Distance of a Coronal Mass Ejection-Driven Shock" *The* ***Astrophysical Journal Letters***, Vol. 736, (2011), https://doi.org/10.1088/2041-8205/736/1/L17.
19. F. Zhang, T. Si, Z. Zhai, X. Luo, J. Yang, and X. Lu, "Reflection of cylindrical converging shock wave over a plane wedge," ***Physics of Fluids,*** Vol. 28, (2016), https://doi.org/10.1063/1.4961069.
20. W. Poomvises, N. Gopalswamy, S. Yashiro, R. Kwon, and O. Olmedo, "Determination of the Heliospheric radial Magnetic Field from the Standoff Distance of a CME-Driven Shock Observed by the Stereo Spacecraft,"

Astrophysical Journal, Vol. 758, (2012), https://doi.org/10.1088/0004-637X/758/2/118.

21. E. Rathakrishnan, "Visualization of the Flow Field Around a Flat Plate," IEEE Instrumentation & Measurement Magazine, Vol. 15, No. 6 (2012): 8-12.
22. S. Khurana and K. Suzuki, "Towards Heat Transfer Control by Aerospikes for Lifting- Body Configuration in Hypersonic Flow," in In 44th AIAA Thermophysics Conference, 2013, https://doi.org/10.2514/6.2013-2898.
23. S. Khurana, K. Suzuki, and E. Rathakrishnan, "Flow field behavior with Reynolds number variance around a spiked body" ***Modern Physics Letters B***, Vol. 30, No. 30, (2016), 1650362.
24. G. Ghassabi and M. Kahrom, "Heat Transfer Enhancement of a Flat Plate Boundary Layer Distributed by a Square Cylinder: Particle Image Velocimetry and Temperature-Sensitive Paint Measurements and Proper Orthogonal Decomposition Analysis," ***International Journal of Engineering, Transactions B: Applications***, Vol. 31, No. 11, (2018), 1962–1971.
25. H. Kazemi, R. Shafaghat, and A. Hajiabadi, "Foil Application to Reduce Resistance of Catamaran under High Speeds and Different Operating Conditions," ***International Journal of Engineering, Transactions A: Basics***, Vol. 32, No. 1, (2019), 106–111.
26. S. M. Umair, N. P. Gulhane, A. R. A. Al-robaian, and S. A. Khan, "On Numerical Investigation of Semi-empirical Relations Representing Local Nusselt Number at Lower Nozzle-target Spacing's," ***International Journal of Engineering, Transactions A: Basics***, Vol. 32, No. 1, (2019), 137–145.
27. A. Ayoub and K. Karamcheti, "An experiment on the flow past a finite circular cylinder at high subcritical and supercritical Reynolds numbers," Journal of Fluid Mechanics, Vol. 118, (1982), 1–26.
28. H. Sharma, A. Vashishtha, and E. Rathakrishnan, "Twin-vortex flow physics," Proceedings of the Institution of Mechanical Engineers, Part G, Vol. 222, No. 6, (2008), 783–788.
29. R. Pinto, A. Afzal, L. D'Souza, Z. Ansari, and A. D. Mohammed Samee, "Computational Fluid Dynamics in Turbomachinery: A Review of State of the Art," ***Archives of Computational Methods in Engineering*** Vol. 24, No. 3, (2017) 467–479.

Determination of Shock Standoff Distance for Wedge at Supersonic Flow

A. Mishra[a], A. Khan[b], N. Musfirah Mazlan[b]

[a] *Department of Aerospace Engineering, IIT Kanpur, India*
[b] *School of Aerospace Engineering, Engineering Campus, Universiti Sains Malaysia, Pulau Pinang, Malaysia*

PAPER INFO

Paper history:
Received 05 February 2019
Received in revised form 12 March 2019
Accepted 02 May 2019

Keywords:
Flow Channel
Shock Standoff
Supersonic Flow
Wedge

چکیده

یک تحقیق تجربی برای محاسبه فاصله متقابل شوک (SSO) در مقابل یک گوه زاویه حاد انجام شده است. برای این آزمایش، جریان آب در کانال ساده تجزیه و تحلیل انجام گردید. سرعت جریان از ۱۳٫۲ سانتی متر / ثانیه به ۲۵٫۵ سانتی متر / ثانیه افزایش می یابد در مراحل اول سرعت متغیر است. سرعت ۱۳٫۲ cm / s مربوط به عدد فراد Froude ۱٫۱۳ و سرعت ۲۵/۵ سانتی متر بر ثانیه مربوط به عدد فراد Froude=1.41 می باشد. اعداد Froude از ۱٫۱۳ به ۱٫٤۱ با اینکرومت ۰٫۰٤ رسیده است. این مطالعه بر روی صفحات آکریلیک ضخیم ۵ میلیمتر و زاویه های گوه ۵۰، ٦۰ و ۷۵ درجه انجام می شود تا بتواند برای محاسبه فاصله SSO در مورد تعداد فروود، رابطه ای به دست آورد. یافته شده است که فشار بالا به شدت به زاویه و عددFr و گوه بستگی دارد. فاصله SSO به صورت تجربی مشخص شده و با استفاده از همبستگی پیشنهاد شده، در توافق خوب قرار دارد.

***doi**: 10.5829/ije.2019.32.07a.19*